ROYAL SOCIETY OF CHEMISTRY

PAPER

CrossMark
click for updates

Side-chain-type anion exchange membranes bearing pendant quaternary ammonium groups *via* flexible spacers for fuel cells†

Chen Xiao Lin, Xiao Ling Huang, Dong Guo, Qiu Gen Zhang, Ai Mei Zhu, Mei Ling Ye and Qing Lin Liu*

To realize high performance anion exchange membranes (AEMs) for alkaline fuel cells (AFCs), a series of quaternized poly(ether sulfone)s (PESs) with different lengths of flexible spacers linking cationic groups and the backbone was synthesized *via* nucleophilic polycondensation, demethylation and Williamson reactions. Atomic force microscopy (AFM) phase images show clear hydrophilic/hydrophobic phase separation for all the side-chain-type AEMs. The PES-n-QA membrane with hexyleneoxy spacers ($n = 6$) between the cationic groups and backbone (benzene ring) exhibited the maximum conductivity of 62.7 mS cm^{-1} (IEC = 1.48 meq. g^{-1}) at 80 °C. The AEM materials are found to have an improved long-term alkaline stability by extending the length of the flexible spacer ($n \geq 4$). The PES-12-QA membrane with a flexible dodeceneoxy spacer demonstrated the highest alkaline stability, where the conductivity and IEC only decreased by 8.1% and 6.9% after immersing in a 1 M aqueous KOH solution at 60 °C for 720 h. Furthermore, the single fuel cell performance test using PES-6-QA as an AEM showed a maximum power density of 108.3 mW cm^{-2} at a current density of 250 mA cm^{-2} at 60 °C.

Introduction

Fuel cells are considered as one of the most promising power conversion devices for stationary and mobile applications due to their high energy density, high efficiency, and low pollution.[1] During the past few decades, fuel cells based on proton exchange membranes (PEMs) have been the subject of intense research.[2,3] Solid polymer membranes serve as an ion conductor and a barrier for fuels and an oxidant is a critical material for fuel cells. PEMs such as Nafion (Dupont) are the most noted solid polymer membranes due to their high proton conductivity, robust mechanical properties and excellent chemical stability.[4] However, the large-scale commercialization of Nafion-based proton exchange membrane fuel cells (PEMFCs) is impeded by their high fuel permeability and strong dependency on expensive noble metal (*e.g.* Pt) catalysts.[5] Compared with

PEMFCs, alkaline fuel cells (AFCs) based on anion exchange membranes (AEMs) take advantage of faster electrode reaction kinetics for the oxygen reduction reaction under alkaline conditions and enable the use of non-noble metals (such as Co and Ni) instead of precious Pt as electrocatalysts, thus significantly lowering the cost of fuel cell devices.[6,7] Furthermore, fuel permeation was inhibited because the conducting direction of hydroxide ions is opposite to that of fuel crossover.[8] Although AFCs have many advantages, the practical application of solid polymer membranes in AFCs still faces the challenges of low conductivity and poor alkaline stability of most current AEMs.

In recent years, a variety of AEM materials based on poly(sulfone)s,[9,10] poly(arylene ether)s,[11] poly(phenylene oxide)s,[12–14] poly(styrene)s,[15,16] poly(olefin)s,[17,18] and polybenzimidazoles[19,20] have been reported for developing high performance AEMs. In the majority of these reports, AEMs are prepared *via* chloromethylation or bromination, followed by the Menshutkin reaction with tertiary amine. However, there are some disadvantages that limit their use in preparing AEMs. Chloromethyl methyl ether is commonly used for the chloromethylation reaction, but the reagent is carcinogenic and harmful to human health. The bromination of benzylmethyl groups using *N*-bromosuccinimide can avoid the use of toxic reagents, however, the corresponding quaternary ammonium (QA) groups are directly attached to benzyl. This will make the QA groups vulnerable to being attacked by hydroxide ions under alkaline conditions because of the electron-withdrawing effect of the benzene ring.[21] Furthermore, the QA groups are

Department of Chemical & Biochemical Engineering, College of Chemistry & Chemical Engineering, Xiamen University, Xiamen 361005, China. E-mail: qlliu@xmu.edu.cn

† Electronic supplementary information (ESI) available: Quaternization reaction of 1, ω-dibromoalkanes in THF; ^{1}H NMR spectrum of Br-x-QA (x = 3, 4, 6, 8, and 12); ^{1}H NMR spectrum of PES-OCH$_3$ and PES-OH; ^{1}H NMR spectrum of PES-n-QA (n = 3, 4, 6, 8, and 12); the appearance (a and b), SEM images of (c) the cross-section and (d) surface of PES-6-QA; the number of absorbed water molecules around each QA group (λ) as a function of flexible spacer length for PES-n-QA membranes at 30, 60 and 80 °C; ^{1}H NMR spectrum of (a) PES-4-QA, (b) PES-6-QA and (c) PES-8-QA stored in 1 M aqueous KOH solution at 60 °C for 0 and 720 h, respectively; the proposed degradation pathways of QA groups for PES-3-QA under alkaline conditions. See DOI: 10.1039/c6ta05090e

13938 | *J. Mater. Chem. A*, 2016, 4, 13938–13948

This journal is © The Royal Society of Chemistry 2016

connected to the backbone *via* a short link (–CH$_2$–), which will restrict the local mobility of the ion groups and prevent the formation of micro-phase separation morphology which seems to be essential for fabricating highly efficient ion channels.

Recently, a few researchers focused on preparing side-chain-type AEMs bearing long flexible spacers between the backbone and cationic groups since they usually possess a greatly higher alkaline stability and conductivity than those AEMs with benzyl-substituted cations.[22–25] The electron-withdrawing effect on QA groups is weak because the cationic groups are far away from the backbone, which could reduce the degradation of cationic groups. Furthermore, the flexible spacers improve the local mobility of ion groups, which is favourable for fabricating hydrophilic/hydrophobic micro-phase separation morphology and thus enhancing conductivity.[26] However, it is difficult to prepare a polymer structure that contains long flexible side chains linking the cationic groups and the polymer backbone.[27] Thus, AEMs with such a side-chain-type structure were rarely reported. Jannasch *et al.*[22] reported a series of quaternized poly(phenyl oxide)s (PPOs) with QA groups attached to the backbone *via* a long flexible side chain. The hydroxide conductivity and alkaline stability of the membranes were significantly enhanced over the QA groups located in benzylic positions. Nevertheless, chemical grafting using highly flammable *n*-BuLi as the lithiation reagent is tedious which should be carried out under water-free and oxygen-free conditions at a very low temperature (−78 °C). Hence, there is an urgent demand to design a strategy to facilely prepare side-chain-type AEMs with a similar structure. Furthermore, the structure–property relationship, especially the effect of the length of the flexible spacer on the performance of the membrane, which is important for designing AEMs with enhanced conductivity and stability, is unclear.

In the present work, we prepared a series of novel side-chain-type AEMs with various lengths of flexible spacers linking the QA groups and the polymer backbone. In addition, a hydroxyl-bearing poly(ether sulfone) backbone was prepared *via* nucleophilic substitution polycondensation and demethylation reactions, followed by grafting (ω-bromoalkyl)trimethylammonium bromides (Br-*n*-QA) into the backbone to give side-chain-type copolymers. This synthetic strategy avoids the use of highly flammable *n*-BuLi and the chemical grafting process was carried out *via* the Williamson reaction, which is much easier than the lithiation-grafting reaction. Herein, Br-*n*-QA with different lengths of carbon chains was designed to obtain various flexible spacers. In particular, the effect of the length of the flexible spacer between the QA groups and backbone on the properties such as water uptake, swelling ratio, hydroxide conductivity and alkaline stability of the AEMs was investigated systematically.

Experimental

Materials

Bis(4-fluorophenyl) sulfone (FPS) (99.0%), 2-methoxyhydroquinone (MHQ) (98.0%) and 4,4′-(hexafluoroisopropylidene)diphenol (BPHF) (98%) were purchased from Tokyo Chemical Industry Co. Ltd and dried under vacuum at room temperature (RT) overnight before use. Potassium carbonate (K$_2$CO$_3$, 99%), toluene (AR), trimethylamine solution (30% in water), dimethylacetamide (AR) (DMAc), dimethyl sulfoxide (AR) (DMSO) and tetrahydrofuran (AR) (THF) were obtained from Sinopharm Chemical Reagent Co. Ltd and used as received. Boron tribromide (99.9%), 1,3-dibromopropane (98%), 1,4-dibromobutane (98%), 1,6-dibromohexane (97%), 1,8-dibromooctane (98%) and 1,12-dibromododecane (98%) were purchased from Aladdin Chemistry Co. Ltd. Other chemical reagents were obtained from Aladdin and used as purchased.
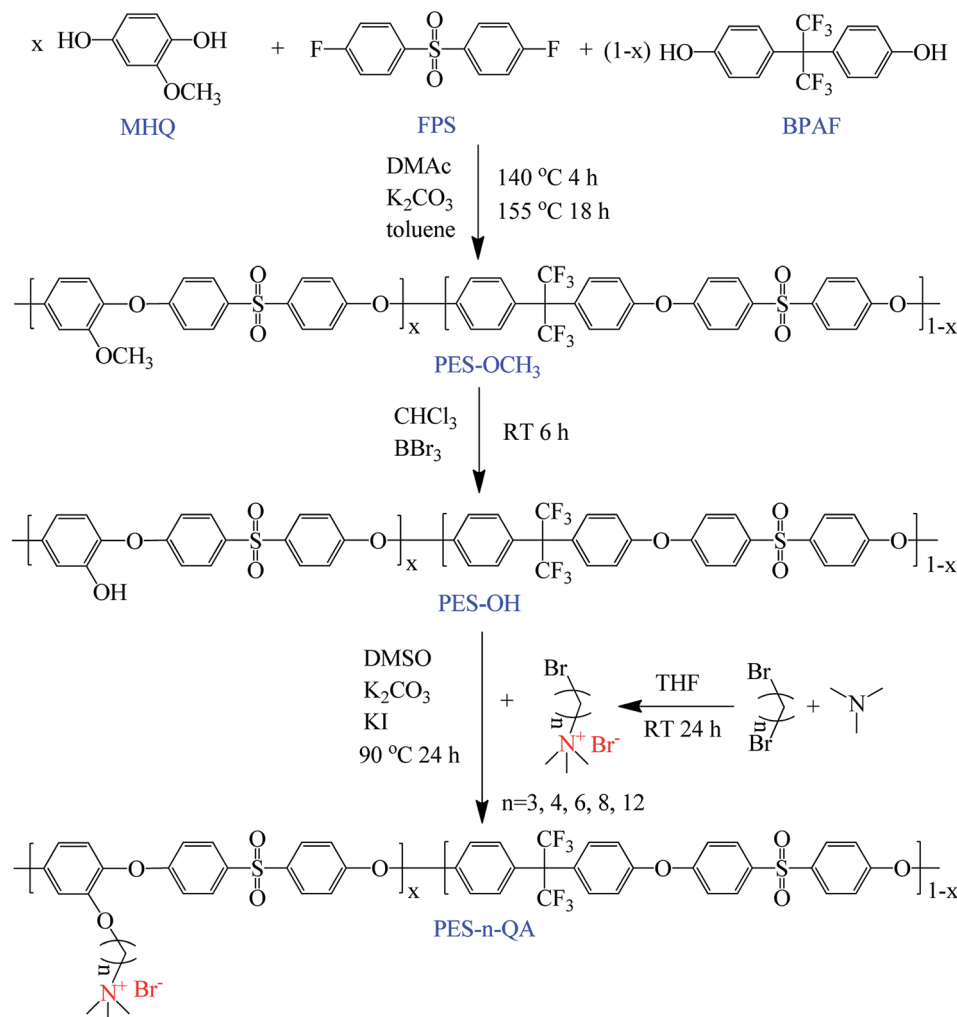
Preparation of side-chain-type AEMs

Synthesis of (ω-bromoalkyl)trimethylammonium bromide (Br-*n*-QA). Br-*n*-QA was synthesized according to the literature with some modifications.[28] The synthetic route for preparing Br-*n*-QA (n = 3, 4, 6, 8 and 12), where n is the number of carbon atoms linking the –Br groups and QA groups, is shown in Scheme 1. Taking Br-6-QA as an example, 24.4 g (100 mmol) of 1,6-dibromohexane and 150 mL of THF were placed into a 500 mL three-necked round-bottom flask equipped with a magnetic stirrer. Trimethylamine gas was produced by heating trimethylamine solution at a certain temperature and then was introduced into the flask at a rate of 12 mL min^{-1} at RT for 4 h through a glass tube which extended below the surface of the reaction solution. The reaction mixture was stirred for another 24 h to obtain a white precipitate. The precipitate was filtered and washed with THF several times, followed by vacuum drying at RT for 24 h to give a product. Br-*n*-QA (n = 3, 4, 8 and 12) was synthesized using the same method. The chemical structure of the products was characterized using ^{1}H NMR spectra in DMSO-d$_6$.

Synthesis of hydroxyl-containing poly(ether sulfone) (PES-OH). PES-OH was synthesized from methoxyl-containing poly(ether sulfone) (PES-OCH$_3$) *via* the demethylation reaction as our previous report.[29] A typical procedure for preparing PES-OCH$_3$ is described as follows (Scheme 1). To a 100 mL three-necked flask equipped with a mechanical stirrer, a condenser, a Dean–Stark trap and a nitrogen inlet/outlet, 5.0850 g of FPS (20 mmol), 1.0087 g of BPHF (3 mmol), 2.3824 g of MHQ (17 mmol), 5.5284 g of K$_2$CO$_3$ (40 mmol), 55 mL of DMAc and 15 mL of toluene were mixed and heated to 140 °C for 4 h, followed by heating up to 155 °C for another 18 h. The reaction mixture was cooled to RT and poured into a large excess of methanol solution to precipitate the copolymers. The product was filtered and washed with methanol thoroughly and dried under vacuum at 80 °C for 24 h (yield: 96%).

For preparing PES-OH, 5.000 g of PAES-OCH$_3$ was dissolved into 100 mL of chloroform to form a solution in a 250 mL three-necked flask with a magnetic stirrer and a nitrogen inlet/outlet. 4 mL of BBr$_3$ was added dropwise into the PAES-OCH$_3$ solution at RT. After reaction for 12 h, the resulting precipitate was filtered and washed thoroughly with a large excess of methanol. Then, the solid was dried under vacuum at 80 °C for 24 h (yield: 88%).

This journal is © The Royal Society of Chemistry 2016

J. Mater. Chem. A, 2016, **4**, 13938–13948 | **13939**

Scheme 1 Synthetic route of Br-n-QA, PES-OCH3, PES-OH and PES-n-QA.

Synthesis of quaternary ammonium-functionalized poly(ether sulfone)s (PES-n-QA). Scheme 1 shows the procedure for preparing PES-n-QA (n = 3, 4, 6, 8 and 12). Typically, the synthesis of PES-6-QA is given as an example. 1 g of PES-OH (2.2858 mmol –OH) and 20 mL of DMSO were placed into a 100 mL round-bottom flask equipped with a magnetic stirrer, a condenser and a gas inlet/outlet. The mixture was heated to 90 °C with stirring until all the polymer was completely dissolved to form a brown homogeneous solution. Then, Br-6-QA (1.0392 g, 3.4287 mmol), K$_2$CO$_3$ (0.6318 g, 4.5716 mmol) and KI (0.0379 g, 0.2283 mmol) were added and the reaction was continued at 90 °C for 24 h. After cooling to RT, the copolymer was precipitated in acetone and washed with acetone and water several times to remove residual DMSO and other salts, followed by vacuum drying at 80 °C for 24 h to yield a light brown solid (yield: 95%).

Fabrication of membranes. The PES-6-QA (1 g) was dissolved in DMF (20 mL) to form a 5 wt% solution. The resulting solution was filtered through a 0.45 μm PTFE syringe filter and was then cast onto four glass plates and dried at 60 °C under vacuum for 24 h to make the PES-6-QA membranes in bromide form. The resulting membranes were peeled off and immersed in a 1 M KOH solution at RT for 48 h to make the hydroxide form PES-6-QA membranes, followed by repeatedly washing with deionized (DI) water to remove any residual free ions and immersing in DI water for more than 48 h before use.

Characterization

^{1}H nuclear magnetic resonance (NMR) spectra were recorded at 500 MHz on a Bruker AV500 spectrometer using tetramethylsilane (TMS) as the internal reference. The molecular weight of the copolymers was determined using a gel permeation chromatography (GPC) system (Waters, USA) using THF as the eluent and polystyrene as the standard. A scanning electron microscope (SEM) (Sigma, Zeiss, Germany) was used to observe the morphology of the membranes. Atomic force microscopy (AFM) images of the AEMs were captured on a DI Multimode V microscope (Bruker Co.) in a tapping mode at ambient temperature with a relative humidity of ~60%. The characterization of the AEMs by small angle X-ray scattering (SAXS) was carried out on a SAXSee-MC2 X-ray diffractometer (Anton Paar,

13940 | *J. Mater. Chem. A*, 2016, **4**, 13938–13948

This journal is © The Royal Society of Chemistry 2016

Austria) under vacuum at RT. The membranes were placed under vacuum at 60 °C for 24 h before measurements.

Measurements

Ion exchange capacity. Ion exchange capacity (IEC) was measured by both ^{1}H NMR spectroscopy and the back titration method. A hydroxide form membrane was dried under vacuum at 80 °C for 24 h and then immersed in 30 mL of a 0.1 M HCl standard solution for 48 h. Subsequently, the solution was neutralized with a 0.1 M KOH solution using phenolphthalein as the indicator. The IEC of the membranes can be calculated from eqn (1).

$$IEC = \frac{M_1 - M_2}{m} \quad (1)$$

where m (g) is the weight of the dry membranes, and M_1 and M_2 are the initial and final amount of H$^+$ in the HCl solution, respectively.

Water uptake and the swelling ratio. Water uptake and the swelling ratio were measured after drying the hydroxide form membranes under vacuum at 80 °C for 24 h. The dried membranes were immersed in DI water at a certain temperature for 24 h. Subsequently, the mass and length/thickness of the membranes were recorded. The water uptake of the membranes is calculated by

$$WU = \frac{m_w - m_d}{m_d} \times 100\% \quad (2)$$

where m_d is the mass of the dry membranes and m_w is the mass of the wet membranes. The number of absorbed water molecules around each QA group (λ) is calculated by

$$\lambda = \frac{WU(\%) \times 10}{IEC \times 18} \quad (3)$$

The in-plane and through-plane swelling of the membranes is estimated by the difference between the wet and dry dimensions in the length or thickness direction, which can be calculated by

$$SR_{in\text{-}plane} = \frac{L_w - L_d}{L_d} \times 100\% \quad (4)$$

$$SR_{through\text{-}plane} = \frac{T_w - T_d}{T_d} \times 100\% \quad (5)$$

where L_w and L_d are the length of the wet and dry membranes, and T_w and T_d are the thickness of the wet and dry membranes, respectively.

Hydroxide conductivity. The hydroxide conductivity (σ, mS cm^{-1}) of the membrane sample (size: 1 cm × 3 cm) is calculated by

$$\sigma = \frac{d}{AR} \quad (6)$$

where d is the distance between the reference electrodes (here 1 cm), and A is the cross-sectional area of the membrane (cm^2). The membrane impedance R (kΩ) was recorded on a Parstat 263 electrochemical workstation (Princeton Advanced Technology,

USA) over the frequency range from 0.1 Hz to 100 kHz using the two-point probe alternating current technique. The hydroxide conductivity measurements were carried out under a fully hydrated condition by placing the cell into DI water (degassing treatment) to equilibrate at least for 2 h and then to record the impedance spectrum.

Water state analysis. The water state of the AEMs was studied using a low temperature differential scanning calorimeter (DSC; HT-DSC 404, Netzsch, Germany). Before measurement, the excess water in the surface of the fully hydrated membrane samples was removed. The membrane sample was cooled to −20 °C and then heated to 20 °C with a heating rate of 5 °C min^{-1}. The amount of free water can be calculated by the integral area of the endothermic peaks near 0 °C using the fusion enthalpy of water (334 J g^{-1}).[30,31] The amount of bound water can be calculated by subtracting the free water from the total amount of water.

Mechanical properties and thermal stability. Mechanical properties were measured on an Instron 3343 universal testing machine with a stretching rate of 5 mm min^{-1} under ambient conditions. The membrane samples were cut into a dog-bone-shape (5.0 mm × 2.0 mm in the gauge area). The wet membranes were obtained by keeping them in DI water for at least 24 h.

The thermal decomposition of the membrane samples was investigated on a thermogravimetric analyzer (SDT-Q600, TA instruments, USA). Prior to measurements, the samples were dried in an oven under vacuum at 120 °C to a constant weight. The thermal decomposition data were recorded in the temperature range from 50 to 700 °C at a heating rate of 10 °C min^{-1} under a nitrogen atmosphere.

Alkaline stability. The alkaline stability of the AEMs was determined by immersing the membrane samples into a 1 M aqueous KOH solution at 60 °C. During the test, the hydroxide conductivity and ^{1}H NMR spectra were monitored. Prior to measurements, the membranes were washed with DI water and kept in DI water at RT for at least 48 h to remove residual KOH solution.

Membrane electrode assembly fabrication and fuel cell performance

The catalyst ink was prepared by mixing the Pt/C catalyst (40 wt%, Johnson Matthey Co.) with PES-6-QA ionomer solution (5 wt%), water and ethanol. The mass ratio of the dried ionomer to catalyst was controlled to be 2 : 8. Afterward, the catalyst inks were sprayed onto both sides of the PES-6-QA membrane with a thickness of 45 μm to prepare the catalyst-coated membranes (CCMs). The Pt loading in both the anode and cathode was 0.5 mg cm^{-2}. The effective area of the electrodes was 4 cm^2. The resulting CCMs were sandwiched between two pieces of carbon paper (Toray TGP-H-060, Japan), followed by hot-pressing at 5 MPa and RT for 5 min to fabricate the membrane electrode assembly (MEA). The H$_2$/O$_2$ fuel cell performance of the MEA was tested on a fuel cell test system at 60 °C. The flow rate of fully humidified H$_2$ and O$_2$ gases was controlled at 100 mL min^{-1}.

Results and discussion

Synthesis and characterization of Br-*n*-QA and copolymers

(ω-Bromoalkyl)trimethylammonium bromide (Br-*n*-QA) was synthesized by the Menshutkin reaction of 1,ω-dibromoalkanes with trimethylamine. Usually, the quaternization reaction can take place at both ends of the 1,ω-dibromoalkanes depending on the reagents and reaction conditions.[20,28] In the present work, the quaternization reaction occurred exclusively at one end of 1, ω-dibromoalkane using THF as the solvent, in which Br-*n*-QA precipitated from the solution when it was formed and thus prevented the formation of the di-quaternized by-product. The ^{1}H NMR spectroscopy analysis (Fig. S1, ESI†) indicated that Br-*n*-QA was obtained with a yield ranging from 56% to 68% (Table S1†) without the di-quaternized by-product. Taking Br-6-QA as an example (Fig. S1(c)†), the peak around 3.1 ppm is attributed to the –CH₃ in the QA groups. The peaks around 3.3 and 3.5 ppm are assignable to the first –CH₂– next to the QA groups and –Br groups, respectively. Additionally, the signals at 1.3, 1.4, 1.7 and 1.8 ppm are attributed to the chemical shifts of other –CH₂– groups in the alkyl chain. The integration ratio of H4 to H1 was 4.50 and agreed well with the theoretical value of 4.50, confirming the successful synthesis of Br-6-QA without a di-quaternized by-product. All other well-assigned ^{1}H NMR spectra (Fig. S1†) confirmed the chemical structure of Br-*n*-QA. A nucleophilic polycondensation reaction (Scheme 1) was used to synthesize PES-OCH₃ with a high molecular weight (M_n = 47 kg mol⁻¹ and M_w = 73 kg mol⁻¹). The demethylation reaction of PES-OCH₃ using BBr₃ as the demethylation reagent was carried out in chloroform as our previous report,[29] and was confirmed by ^{1}H NMR spectroscopy analysis. As shown in Fig. S2,† all the peaks ranging from 6.6 to 8.0 ppm are attributed to the aromatic protons on the benzene rings. The peak around 3.7 ppm associated with proton signals from –OCH₃ groups disappeared after the demethylation reaction and a new peak at around 10.1 ppm attributed to the phenolic-OH groups appeared. This confirms the successful synthesis of PES-OH.

The side-chain-type PES-*n*-QA copolymers were synthesized by grafting Br-*n*-QA into the poly(ether sulfone) backbone (PES-OH) *via* a Williamson reaction (Scheme 1). An excess of Br-*n*-QA was used to enhance the grafting degree. The ^{1}H NMR spectra of PES-*n*-QA are shown in Fig. S3.† Taking PES-6-QA as an example (Fig. S3(c)†), the disappearance of the proton resonance arising from the phenolic-OH groups as a sharp peak around 10.1 ppm along with the appearance of new peaks at 0.8–1.8 ppm and 3.0–4.0 ppm attributed to proton resonance from the quaternary ammonium side chain demonstrated that Br-6-QA was grafted into the poly(ether sulfone) backbone successfully. The integral ratio of the peaks from the QA groups to aromatic proton peaks was in good accordance with the one calculated from the feed ratio, indicating the near-quantitative reaction of the phenolic-OH groups. The ion exchange capacity (IEC) measured by back-titration agreed well with that calculated from ^{1}H NMR spectroscopy analysis (Table 1), indicating that Br⁻ was mostly replaced by OH⁻.

Morphological characterization

Taking PES-6-QA as an example, transparent and flexible membranes were prepared by dissolving the ionic copolymers in DMF and casting them on a flat Teflon sheet (Fig. S4(a) and (b)†). The morphology of the as-synthesized AEMs was observed using SEM, as shown in Fig. S4(c) and (d).† It is seen that a smooth, homogeneous and dense membrane without pores is formed after exchanging to the hydroxide form.

Atomic force microscopy (AFM) was employed to further reveal the morphology of the AEMs. The AFM phase images of the PES-*n*-QA membranes with various side chains were recorded in a tapping mode at ambient temperature. As shown in Fig. 1(a)–(e), the darker regions represent hydrophilic (ionic) domains, whereas the brighter ones represent hydrophobic domains.[19] Clear hydrophilic/hydrophobic phase separation was observed for all of the AEMs. It should be noted that the hydrophobic poly(ether sulfone) backbone is immiscible with the hydrophilic side chain, thus driving side-chain-type copolymers to self-assemble and fabricate hydrophilic nano-channels containing QA groups and water, which is beneficial for conducting hydroxide ions.[32,33] The largest hydrophilic domain was observed for PES-6-QA with hexyleneoxy spacers, and not for those with shorter or longer spacers. It may be that if $n \leq 6$ the enhanced local mobility of cationic groups is beneficial for facilitating micro-phase separation, while the hydrophobic alkyl chain between the backbone and QA groups becomes too long ($n \geq 6$), the decreased hydrophilicity of the side chain may result in the weakening of the hydrophilic/hydrophobic phase separation degree. Hence, PES-6-QA exhibited more distinct micro-phase separation than other membranes. In the SAXS

Table 1 IEC, water uptake, swelling ratio and λ of the PES-*n*-QA membranes

| Membrane | IEC (meq. g⁻¹) | | | Water uptake[d] (%) | Swelling ratio[d] (%) | | λ[d] |
	Theo.[a]	Cal.[b]	Exp.[c]		In-plane	Through-plane	
PES-3-QA	1.62	1.60	1.58 ± 0.03	53.0 ± 0.9	20.1 ± 0.3	25.7 ± 0.5	18.6
PES-4-QA	1.58	1.56	1.55 ± 0.05	59.4 ± 1.1	21.0 ± 0.4	28.1 ± 0.3	21.3
PES-6-QA	1.51	1.51	1.48 ± 0.03	77.5 ± 1.0	22.0 ± 0.3	29.4 ± 0.4	29.1
PES-8-QA	1.45	1.44	1.42 ± 0.04	58.7 ± 0.9	19.7 ± 0.5	23.3 ± 0.4	23.0
PES-12-QA	1.34	1.34	1.31 ± 0.04	44.0 ± 0.5	15.5 ± 0.4	17.9 ± 0.3	18.7

[a] Calculated from the monomer ratio. [b] Calculated from ^{1}H NMR spectra. [c] Measured by back titration. [d] Determined at 30 °C; an average of three measurements.

13942 | *J. Mater. Chem. A*, 2016, **4**, 13938–13948

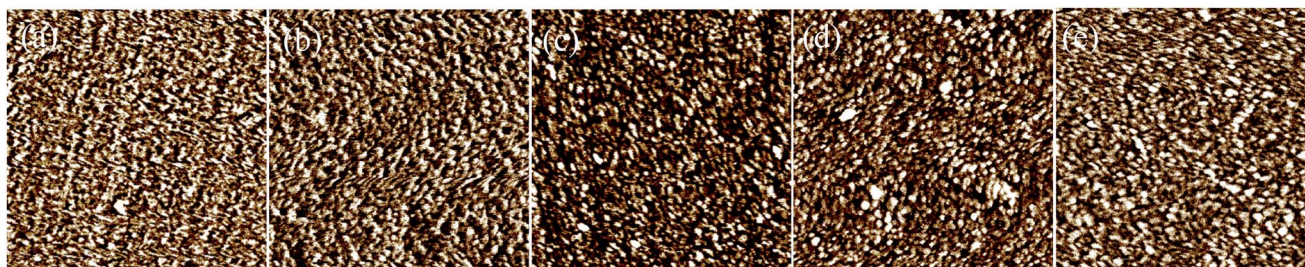This journal is © The Royal Society of Chemistry 2016

Fig. 1 AFM phase images of (a) PES-3-QA, (b) PES-4-QA, (c) PES-6-QA, (d) PES-8-QA and (e) PES-12-QA. Scan box: 500 nm × 500 nm.
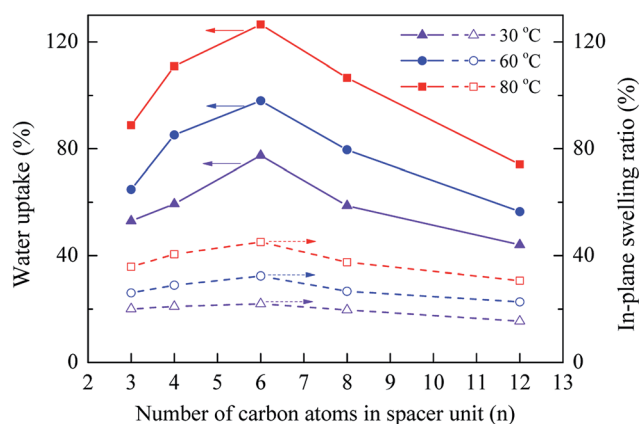

Fig. 2 Water uptake and the swelling ratio as a function of flexible spacer length for PES-n-QA membranes at 30, 60 and 80 °C.

results, however, no obvious scattering peak was found for the membranes (Fig. S5†). It should be noted that the poly(ether sulfone)-based materials are inherent with the semi-crystalline nature and display no or weaker characteristic peaks in SAXS than the crystalline polymers such as poly(phenylene oxide) derivatives,[22,32–34] but the AFM phase images were clear enough to conduct the morphological analysis for the side-chain-type AEMs. As shown below, the phase separation morphology has a strong effect on the hydroxide conductivity.

Water uptake and swelling behaviour

Fig. 2 shows the water uptake and in-plane swelling ratio of the PES-n-QA membranes in hydroxide form after immersing in water at 30, 60 and 80 °C. As expected, the water uptake of all the membranes increased with temperature. It is clearly found that the water uptake depends strongly on the length of the flexible spacer linking the QA groups and backbone. On increasing the length of the flexible spacer, an increase in water uptake was observed for $n \leq 6$ and a decrease in water uptake was observed for $6 \leq n \leq 12$. A maximum value was achieved to be 77.5% at 30 °C and 126.5% at 80 °C for PES-6-QA with hexyleneoxy as the flexible spacer. It is plausible that the hydrophobicity of the membranes enhanced greatly by introducing many more methylene groups into the side chain, which restricted the water uptake of PES-8-QA and PES-12-QA.[23] In addition, the number of absorbed water molecules per QA group (designated as λ) was calculated to overcome the IEC differences of the AEMs. As shown in Table 1

and Fig. S6,† the tendency of λ is in accordance with water uptake and the value ranges from 18.6 to 29.1 at 30 °C.

The water in the AEMs is critical for ion dissociation and fabricating hydroxide conducting channels. The water in the membranes can be generally classified into two kinds: free water and bound water.[30] We use DSC to obtain the amount of free water in the membrane because the free water exhibits a melting point near 0 °C,[35] and the DSC curves are shown in Fig. S7.† In order to analyse the content of free/bound water, the hydration number was calculated and is presented in Fig. S8.† The AEMs exhibit a similar content of bound water near the QA groups while the tendency for the content of free water is in line with water uptake. The highest content of free water was obtained by the PES-6-QA membrane. As shown below, the water content in the membrane will have a great influence on the hydroxide conductivity.

To demonstrate the influence of the length of the flexible spacer on the swelling behaviour of the AEMs, we compared the in-plane swelling ratio of the PES-n-QA membranes at different temperatures (Fig. 2). It is observed that the tendency of the swelling ratio clearly followed the water uptake. The swelling ratio increased with increasing the length of the flexible spacer when $n \leq 6$. However, the AEMs with a longer flexible spacer ($n = 8$ and 12) exhibit a lower swelling ratio than PES-6-QA. For example, the in-plane swelling ratio of PES-6-QA is 22.0% at 30 °C, and is higher than that of PES-8-QA (19.7%) and PES-12-QA (15.5%) at 30 °C. This can be attributed to the increased hydrophobicity by introducing many more methylene groups into the flexible spacer that restrict water adsorption and thus inhibit the swelling. Additionally, Table 1 shows the dimensional swelling in the in-plane and thickness directions at 30 °C. The through-plane swelling ratio of the PES-n-QA membranes is found to be ~1.35-fold higher than the in-plane swelling ratio indicating a mild degree of anisotropy.

It is necessary to maintain a balanced water uptake because too much water will result in high swelling and thus decrease the mechanical properties of the AEMs. All the side-chain-type AEMs show a moderate water uptake and swelling ratio indicating that these membranes can meet the demands of MEA application and fuel cell operation.

Hydroxide conductivity

The conductivity of the AEMs was measured under a fully hydrated condition. Fig. 3(a) shows the temperature
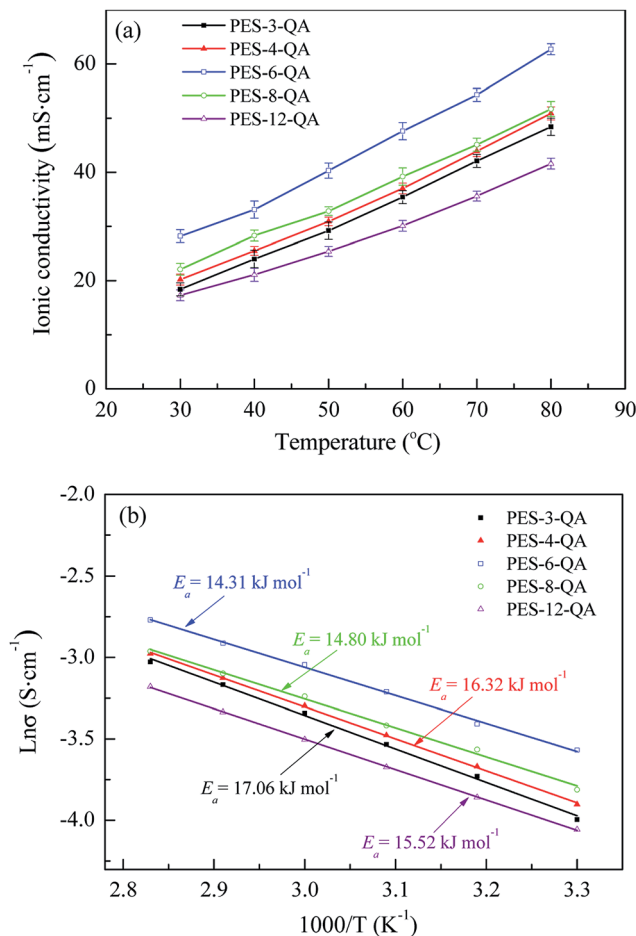
This journal is © The Royal Society of Chemistry 2016

J. Mater. Chem. A, 2016, **4**, 13938–13948 | **13943**

Fig. 4 Hydroxide conductivity as a function of spacer length for the PES-*n*-QA membranes at 30, 60 and 80 °C.

Fig. 3 (a) Temperature dependence of the conductivity of the PES-*n*-QA membranes and (b) their Arrhenius plots.

clear that the optimum hydroxide conductivity was achieved when the spacer between the QA groups and backbone (benzene ring) was hexyleneoxy (PES-6-QA). This may be attributed to the high content of free water in the PES-6-QA membrane due to which the hydroxide ion migration was greatly enhanced.

For a good comparison of the hydroxide conductivity with that of other AEMs, the relative hydroxide conductivity (designated as η = conductivity/IEC) was calculated to overcome the IEC difference. Fig. 5 shows that the PES-*n*-QA membranes have higher relative hydroxide conductivity than some main-chain-type AEMs (QPPO-2, PES-B100-C1 and QPAEK-0.6)[39–41] and some side-chain-type AEMs (SEBS-DMHA and PES-10-PPO).[29,42] The η of the PES-6-QA and PES-80-QA membranes is even higher than that of some block copolymer AEMs (bQAPDHTPE 25, QPAE-X25Y21 and QBPES-40),[43–45] indicating that side-chain-type AEMs bearing flexible pendant QA groups are beneficial for enhancing hydroxide conductivity.

dependence of the conductivity of the AEMs in hydroxide form. The tendency of hydroxide conductivity is found to be similar to water uptake, suggesting that ion transport is strongly dependent on the water content in the membranes. As expected, the conductivity increased with temperature in the range from 30 to 80 °C. This is attributed to the development of saturation of the ion transport channels as the water content of the membranes increased with temperature. As shown in Fig. 3(b), the hydroxide transport activation energies (E_a) of the AEMs are in the range from 14.31 to 17.06 kJ mol^{-1}, and are similar to those of the reported AEMs.[36–38] The lowest E_a of PES-6-QA suggests that the lowest energy is required for ion conduction in the membrane. Fig. 4 shows the conductivity *versus* the spacer linking the backbone and QA groups at 30, 60 and 80 °C. The PES-6-QA membrane (IEC = 1.48 mmol g^{-1}) with hexyleneoxy spacers between the cationic groups and backbone showed the highest conductivity of 62.7 mS cm^{-1} at 80 °C, followed by the PES-8-QA membrane with octyleneoxy spacers. However, the AEMs with a spacer of propyleneoxy (PES-3-QA) and dodecyleneoxy (PES-12-QA) showed the lowest hydroxide conductivity. The lower conductivity may be attributed to the lower water uptake in the membranes, in which the formation of ion conducting channels is hard, as confirmed by AFM (Fig. 1). It is
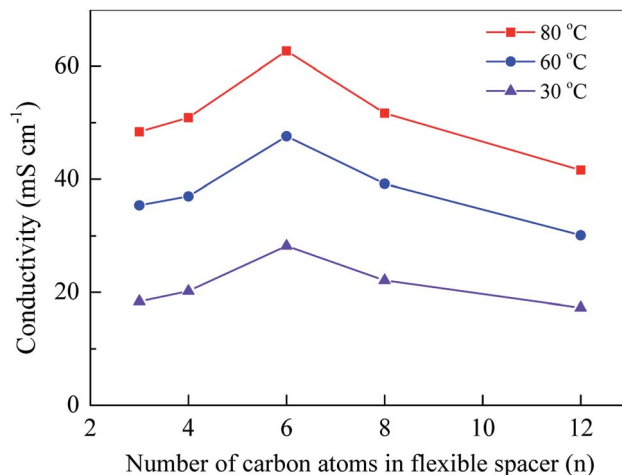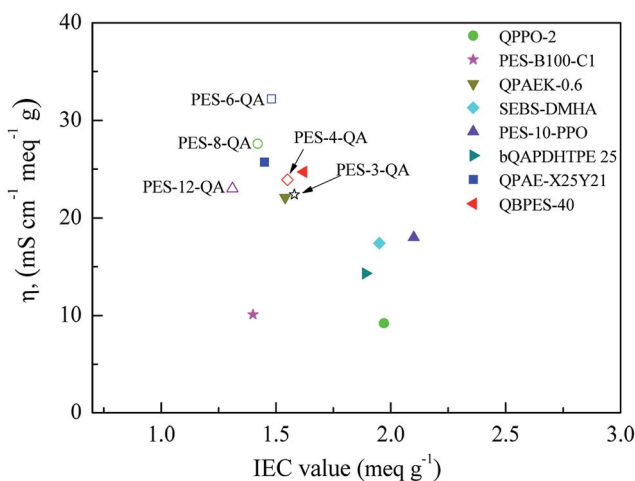

Fig. 5 Relative hydroxide conductivity as a function of IEC for PES-*n*-QA and reported AEMs at 60 °C.

Mechanical properties and thermal stability

The thermal stability of the PES-n-QA membranes in hydroxide form was examined *via* thermogravimetric analysis (TGA) under a nitrogen atmosphere at a heating rate of 10 °C min^{-1} up to 700 °C. As shown in Fig. 6, the membranes show a two-step degradation process. The first step between 150 and 350 °C originated from the degradation of the QA groups in the side chain. The second step above 350 °C was probably due to the degradation of the copolymer backbone. The degradation temperature of all the membranes was far above the operating temperature (roughly 23–70 °C) of alkaline fuel cells. This suggests that the as-synthesized membranes have a good thermal stability.[46]

The mechanical properties of AEMs are critical for fabricating robust MEAs and long-term stability of membranes for fuel cells. The mechanical properties of the wet membranes are important because AEMs are usually in operation under fully hydrated conditions. Thus, the membrane samples were immersed in DI water for at least 24 h before the test. Table 2 shows the mechanical properties of the wet membranes. The tensile strength, Young's modulus and elongation at break of the AEMs were in the range of 9.2–13.6 MPa, 158–285 MPa and 23.3–57.6%, respectively. The PES-n-QA membranes retained adequate tensile strength and could meet the mechanical property requirements for the fabrication of MEAs and application in alkaline fuel cells.

Alkaline stability

AEMs with long-term stability under alkaline conditions are of great importance for fuel cell applications. In the present work, the evaluation of the long-term alkaline stability of the side-chain-type AEMs with various flexible spacers between the backbone and QA groups was performed by immersing the membrane samples in a 1 M aqueous KOH solution at 60 °C for 720 h. It is known that QA groups have a tendency to degrade in a basic environment due to the nucleophilic substitution by the attack of hydroxide ions and/or β-hydrogen (Hofmann) elimination, leading to a decrease in IEC and conductivity.[33,47] Fig. 7

Table 2   Mechanical properties of the membranes in the wet state

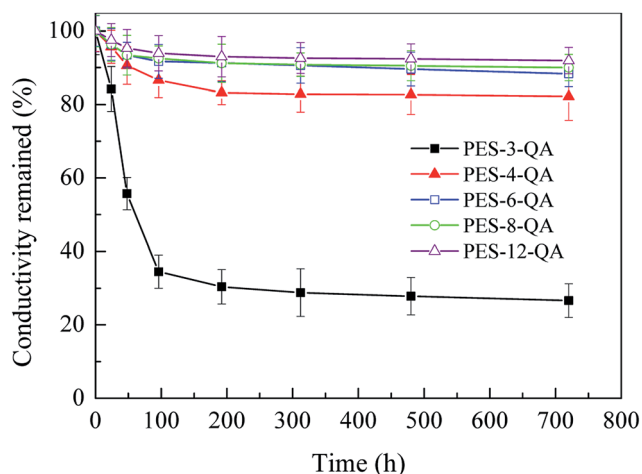| Membrane	Tensile strength (MPa)	Young's modulus (MPa)	Elongation at break (%)
PES-3-QA	13.6 ± 2.1	285 ± 15	28.0 ± 3.2
PES-4-QA	11.5 ± 1.9	219 ± 20	42.1 ± 4.6
PES-6-QA	9.2 ± 1.9	158 ± 12	57.6 ± 3.5
PES-8-QA	11.2 ± 2.2	199 ± 16	38.6 ± 2.8
PES-12-QA	13.1 ± 2.5	270 ± 20	23.8 ± 2.9

Fig. 7   Hydroxide conductivity changes of the PES-n-QA (n = 3, 4, 6, 8, and 12) membranes in a 1 M KOH solution at 60 °C.

shows the change in conductivity during stability testing. Moreover, the IEC and conductivity of the membranes before and after the stability test are given in Table 3. Extending the length of the flexible spacer ($n \geq 4$) results in an improved long-term alkaline stability of AEM materials. As shown in Fig. 7, all the AEMs with the exception of PES-3-QA retained above 80% of their initial conductivity after 720 h of the test. For example, the PES-12-QA membrane demonstrated the greatest alkaline stability, where the conductivity and IEC only decreased by 8.1% and 6.9%, respectively. However, the IEC of PES-3-QA decreased from 1.58 to 0.49 meq. g^{-1}, and the conductivity decreased from 18.4 to 4.9 mS cm^{-1} at 30 °C, and retained only 26.6% and 31.0% of the initial value, respectively. Table S2† shows the mechanical properties after the alkaline stability test. A slight decrease in the tensile strength over the pristine membrane was observed. This indicates that the poly(ether sulfone) backbone may be degraded slightly during the test.

^{1}H NMR spectra (Fig. 8 and S9†) were further used to examine the change in the chemical structure of the membranes. The length of the flexible spacer is found to have a great influence on the alkaline tolerance of the AEMs. As shown in Fig. 8(a) for PES-3-QA, the signal at 3.0 ppm assigned to the QA methyl protons was much weaker than that of the pristine membrane. The two obvious new peaks around 4.9 and 5.7 ppm were attributed to the proton resonance from
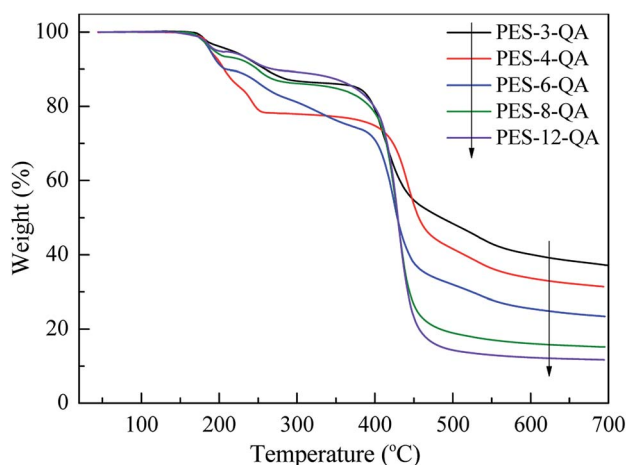

Fig. 6   TGA curves of the PES-n-QA membranes under nitrogen flow.

Table 3 IEC and conductivity of the AEMs before and after immersing in a 1 M KOH solution at 60 °C for 720 h

Membrane	IEC[a] (meq. g^{-1})		Conductivity[b] (mS cm^{-1})	
	Before	After	Before	After
PES-3-QA	1.58	0.49	18.4	4.9
PES-4-QA	1.55	1.36	20.2	16.6
PES-6-QA	1.48	1.33	28.2	24.9
PES-8-QA	1.42	1.30	22.1	19.9
PES-12-QA	1.31	1.22	17.3	15.9

[a] Estimated by back titration. [b] Measured at 30 °C.
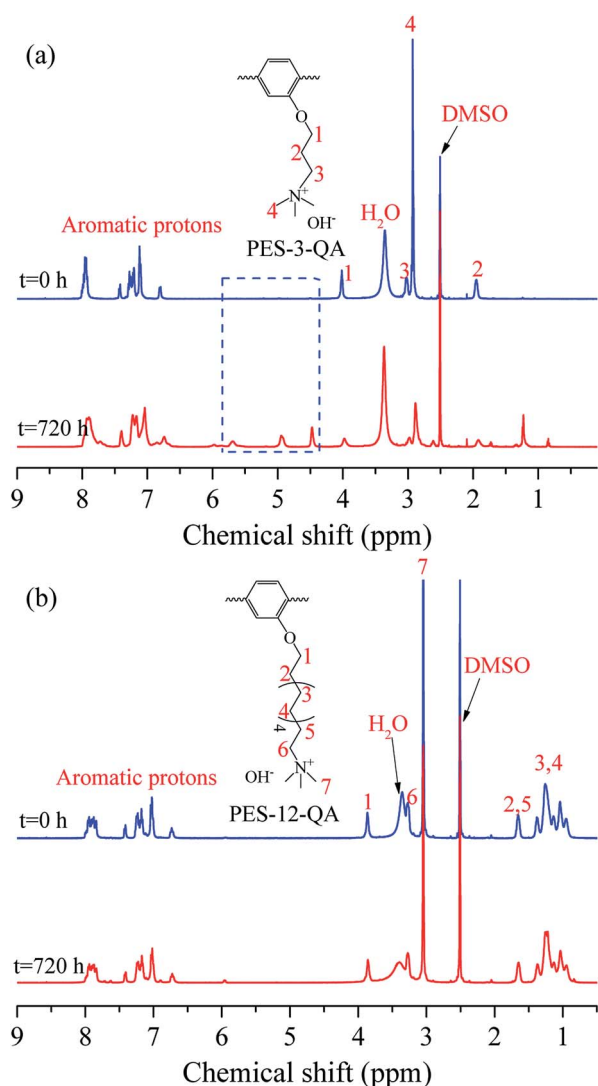
Fig. 8 ^{1}H NMR spectra of (a) PES-3-QA and (b) PES-12-QA stored in a 1 M aqueous KOH solution at 60 °C for 0 and 720 h, respectively.

–CH=CH$_2$. This indicates that the decomposition takes place *via* Hofmann elimination. The new peaks around 0.8, 1.25 and 2.6 ppm may be attributed to the proton resonance from the

product of the nucleophilic substitution reaction. A small peak around 6.0 ppm may be ascribed to the degradation products of the poly(ether sulfone) backbone. Above all, the decrease in IEC and conductivity mainly comes from the degradation of the QA groups. As noted by Elabd *et al.*,[48] the proposed degradation pathways of QA groups for PES-3-QA are presented in Scheme S1.† It is suggested that the presence of the three carbon atoms between the QA groups and the electronegative ether oxygen groups increased the reactivity of β-hydrogen, which will result in the Hofmann elimination reaction.[49] However, there are not any new peaks from 4.3 to 5.8 ppm observed in other ^{1}H NMR spectra of the AEMs after 720 h of the test, indicating that the Hofmann elimination reaction was greatly inhibited *via* extending the length of flexible spacers ($n \geq 4$) linking the QA groups and backbone. The present findings are in accordance with those of Pivovar *et al.*[50] who used the density functional theory (DFT) method to investigate the degradation pathways of ammonium cations with different lengths of carbon chains. There is linkage of the C–C or C–O bond between the QA groups and backbone. Although the linkage of the C–C bond between the QA groups and backbone[24] shows higher alkaline tolerance than the linkage of the C–O bond when the length of alkyl groups is short ($n \leq 3$), the alkaline stability of the AEMs with the C–O bond can be greatly enhanced and is close to the membrane with the C–C bond by extending the flexible spacer ($n \geq 4$). When the length of alkyl groups linking the backbone and QA groups is sufficiently long ($n \geq 4$), the effect of the C–C or C–O group, which is far away from the QA groups, can be negligible. They found that the ammonium is vulnerable to take Hofmann elimination when the carbon chain of alkyl-trimethylammonium cations extended from 2 to 4 and became stable when extended from 4 to 6, which is in line with our results. In addition, the PES-4-QA (Fig. S9(a)†), PES-6-QA (Fig. S9(b)†), PES-8-QA (Fig. S9(c)†) and PES-12-QA (Fig. 8(b)) membranes exhibited a slight decrease of the signal intensity from the QA groups, and demonstrated an excellent stability under alkaline conditions at 60 °C. This is attributed to the increased electron density around β-hydrogen by increasing the number of carbon atoms between the backbone and QA groups, which depressed the electron-withdrawing effect. As a result, the QA groups become less susceptible to being attacked by hydroxide ions. In summary, the cation stability can be greatly improved by increasing the length of the flexible spacer ($n \geq 4$) between the backbone and QA groups.

Single fuel cell performance

The PES-6-QA membrane was evaluated in a single alkaline fuel cell to examine the applicability of the AEMs due to its high conductivity and excellent alkaline stability. The testing was carried out under humidified H$_2$ and O$_2$ with a gas flow rate of 100 mL min^{-1}. Fig. 9 shows the polarization curve of the MEA at 60 and 80 °C. The open circuit voltage (OCV) of the fuel cells is above 1.0 V, and is in the range of typical alkaline fuel cells,[51,52] indicating that the voltage loss caused by gas crossover is insignificant. The maximum power density (P_{max}) of the PES-6-QA membrane at 60 °C was 108.3 mW cm^{-2} at a current density of
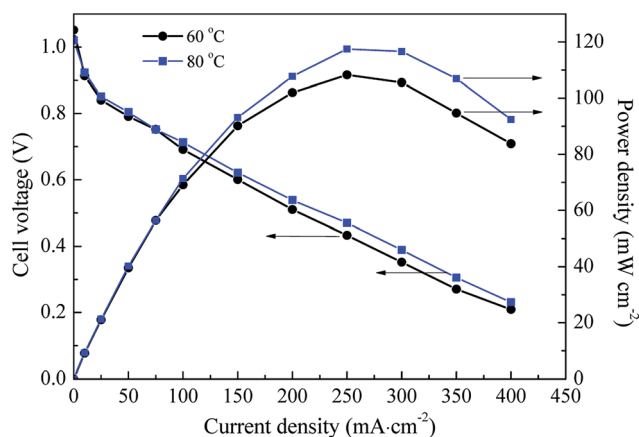
13946 | *J. Mater. Chem. A*, 2016, **4**, 13938–13948

This journal is © The Royal Society of Chemistry 2016

Fig. 9 Fuel cell performance of the MEA using the PES-6-QA membrane at 60 and 80 °C.

250 mA cm^{-2} and is much higher than the P_{max} (42.5 mW cm^{-2}) using QA functionalized copolymers and P_{max} (30 mW cm^{-2}) using an imidazolium-functionalized PPO membrane at 60 °C.[12,53] Furthermore, the PES-6-QA membrane exhibited higher P_{max} (117.5 mW cm^{-2} at a current density of 250 mA cm^{-2}) at 80 °C than that at 60 °C. This is attributed to the increased conductivity of the membrane at elevated temperatures. This suggests that the side-chain-type membranes hold promise for application in alkaline fuel cells. Optimization of the MEA construction and operational conditions is underway in our lab.

Conclusions

In summary, poly(ether sulfone)s bearing pendant quaternary ammonium groups via various lengths of flexible spacers were prepared via nucleophilic polycondensation, demethylation and Williamson reactions. All the AEMs exhibit clear micro-phase separation morphology due to the immiscibility between the hydrophilic side chain and the hydrophobic backbone. It is observed that the length of the flexible spacer linking the cationic groups and backbone has a great influence on the performance of AEMs. The optimum conductivity (62.7 mS cm^{-1}, 80 °C) was observed for PES-6-QA with hexyleneoxy spacers, suggesting that too long alkyl groups in the side chain will increase the hydrophobicity of the membrane, which is bad for fabricating highly efficient ion conducting channels due to the reduced water content. The Hofmann degradation of QA groups in the membrane can be inhibited by increasing the length of the flexible spacer ($n \geq 4$) between the backbone and QA groups. The PES-12-QA membrane demonstrated the highest stability after immersing in a 1 M aqueous KOH solution at 60 °C for 720 h. The single cell test showed a moderate performance of the PES-6-QA membrane, which holds promise for application in alkaline fuel cells.

Acknowledgements

Notes and references

1 Y. J. Wang, J. Qiao, R. Baker and J. Zhang, *Chem. Soc. Rev.*, 2013, **42**, 5768–5787.

2 G. He, Z. Li, J. Zhao, S. Wang, H. Wu, M. D. Guiver and Z. Jiang, *Adv. Mater.*, 2015, **27**, 5280–5295.

3 A. K. Mishra, S. Bose, T. Kuila, N. H. Kim and J. H. Lee, *Prog. Polym. Sci.*, 2012, **37**, 842–869.

4 J. Peron, A. Mani, X. Zhao, D. Edwards, M. Adachi, T. Soboleva, Z. Shi, Z. Xie, T. Navessin and S. Holdcroft, *J. Membr. Sci.*, 2010, **356**, 44–51.

5 M. Tanaka, K. Fukasawa, E. Nishino, S. Yamaguchi, K. Yamada, H. Tanaka, B. Bae, K. Miyatake and M. Watanabe, *J. Am. Chem. Soc.*, 2011, **133**, 10646–10654.

6 N. Li and M. D. Guiver, *Macromolecules*, 2014, **47**, 2175–2198.

7 H. Ono, J. Miyake, S. Shimada, M. Uchida and K. Miyatake, *J. Mater. Chem. A*, 2015, **3**, 21779–21788.

8 S. C. Price, X. Ren, A. C. Jackson, Y. Ye, Y. A. Elabd and F. L. Beyer, *Macromolecules*, 2013, **46**, 7332–7340.

9 J. Pan, S. Lu, Y. Li, A. Huang, L. Zhuang and J. Lu, *Adv. Funct. Mater.*, 2010, **20**, 312–319.

10 J. Pan, Y. Li, L. Zhuang and J. Lu, *Chem. Commun.*, 2010, **46**, 8597–8599.

11 N. Yokota, M. Shimada, H. Ono, R. Akiyama, E. Nishino, K. Asazawa, J. Miyake, M. Watanabe and K. Miyatake, *Macromolecules*, 2014, **47**, 8238–8246.

12 J. Ran, L. Wu, J. R. Varcoe, A. L. Ong, S. D. Poynton and T. Xu, *J. Membr. Sci.*, 2012, **415–416**, 242–249.

13 X. Lin, J. R. Varcoe, S. D. Poynton, X. Liang, A. L. Ong, J. Ran, Y. Li and T. Xu, *J. Mater. Chem. A*, 2013, **1**, 7262–7269.

14 X. Lin, X. Liang, S. D. Poynton, J. R. Varcoe, A. L. Ong, J. Ran, Y. Li, Q. Li and T. Xu, *J. Membr. Sci.*, 2013, **443**, 193–200.

15 C. Yang, S. Wang, W. Ma, S. Zhao, Z. Xu and G. Sun, *J. Mater. Chem. A*, 2016, **4**, 3886–3892.

16 C. Yang, S. Wang, W. Ma, L. Jiang and G. Sun, *J. Mater. Chem. A*, 2015, **3**, 8559–8565.

17 Y. Li, Y. Liu, A. M. Savage, F. L. Beyer, S. Seifert, A. M. Herring and D. M. Knauss, *Macromolecules*, 2015, **48**, 6523–6533.

18 M. Zhang, J. Liu, L. An, M. D. Guiver and N. Li, *J. Mater. Chem. A*, 2015, **3**, 12284–21296.

19 L. Zeng, T. S. Zhao, L. An, G. Zhao and X. H. Yan, *J. Membr. Sci.*, 2015, **493**, 340–348.

20 M. P. Kulkarni, T. J. Peckham, O. D. Thomas and S. Holdcroft, *MRS Online Proc. Libr.*, 2014, **1677**, 1–12.

21 Y. He, J. Pan, L. Wu, Y. Zhu, X. Ge, J. Ran, Z. Yang and T. Xu, *Sci. Rep.*, 2015, **5**(13417), 1–7.

22 H. S. Dang, E. A. Weiber and P. Jannasch, *J. Mater. Chem. A*, 2015, **3**, 5280–5284.

23 H. S. Dang and P. Jannasch, *Macromolecules*, 2015, **48**, 5742–5751.

24 Z. Yang, J. Zhou, S. Wang, J. Hou, L. Wu and T. Xu, *J. Mater. Chem. A*, 2015, **3**, 15015–15019.

This journal is © The Royal Society of Chemistry 2016

J. Mater. Chem. A, 2016, **4**, 13938–13948 | 13947

25 W.-H. Lee, Y. S. Kim and C. Bae, *ACS Macro Lett.*, 2015, **4**, 814–818.

26 N. Li, Q. Zhang, C. Wang, Y. M. Lee and M. D. Guiver, *Macromolecules*, 2012, **45**, 2411–2419.

27 J. R. Varcoe, P. Atanassov, D. R. Dekel, A. M. Herring, M. A. Hickner, P. A. Kohl, A. R. Kucernak, W. E. Mustain, K. Nijmeijer and K. Scott, *Energy Environ. Sci.*, 2014, **7**, 3135–3191.

28 R. A. Bartsch, W. Zhao and Z. Y. Zhang, *Synth. Commun.*, 1999, **29**, 2393–2398.

29 C. X. Lin, Y. Z. Zhuo, A. N. Lai, Q. G. Zhang, A. M. Zhu, M. L. Ye and Q. L. Liu, *J. Membr. Sci.*, 2016, **513**, 206–216.

30 H. Jung, K. Fujii, T. Tamaki, H. Ohashi, T. Ito and T. Yamaguchi, *J. Membr. Sci.*, 2011, **373**, 107–111.

31 N. Hara, H. Ohashi, T. Ito and T. Yamaguchi, *J. Phys. Chem. B*, 2009, **113**, 4656–4663.

32 N. W. Li, T. Z. Yan, Z. Li, T. Thurn-Albrecht and W. H. Binder, *Energy Environ. Sci.*, 2012, **5**, 7888–7892.

33 N. Li, Y. Leng, M. A. Hickner and C. Y. Wang, *J. Am. Chem. Soc.*, 2013, **135**, 10124–10133.

34 A. H. Rao, S. Nam and T.-H. Kim, *J. Mater. Chem. A*, 2015, **3**, 8571–8580.

35 H. Jung, H. Ohashi, T. Tamaki and T. Yamaguchi, *Chem. Lett.*, 2013, **42**, 14–16.

36 M. Liu, Z. Wang, J. Mei, J. Xu, L. Xu, H. Han, H. Ni and S. Wang, *J. Membr. Sci.*, 2016, **505**, 138–147.

37 J. Si, S. Lu, X. Xu, S. Peng, R. Xiu and Y. Xiang, *ChemSusChem*, 2014, **7**, 3389–3395.

38 L. C. Jheng, S. L. C. Hsu, B. Y. Lin and Y. L. Hsu, *J. Membr. Sci.*, 2014, **460**, 160–170.

39 Q. Li, L. Liu, Q. Miao, B. Jin and R. Bai, *Polym. Chem.*, 2014, **5**, 2208–2213.

40 C. X. Lin, Y. Z. Zhuo, A. N. Lai, Q. G. Zhang, A. M. Zhu and Q. L. Liu, *RSC Adv.*, 2016, **6**, 17269–17279.

41 Z. Zhang, K. Shen, L. Lin and J. Pang, *J. Membr. Sci.*, 2016, **497**, 318–327.

42 A. D. Mohanty, C. Y. Ryu, Y. S. Kim and C. Bae, *Macromolecules*, 2015, **48**, 7085–7095.

43 M. A. Hossain, Y. Lim, S. Lee, H. Jang, S. Choi, Y. Jeon, J. Lim and W. G. Kim, *Int. J. Hydrogen Energy*, 2014, **39**, 2731–2739.

44 X. Li, Y. Yu, Q. Liu and Y. Meng, *J. Membr. Sci.*, 2013, **436**, 202–212.

45 Z. Zhao, J. Wang, S. Li and S. Zhang, *J. Power Sources*, 2011, **196**, 4445–4450.

46 G. Merle, M. Wessling and K. Nijmeijer, *J. Membr. Sci.*, 2011, **377**, 1–35.

47 L. Zhu, J. Pan, Y. Wang, J. Han, L. Zhuang and M. A. Hickner, *Macromolecules*, 2016, **49**, 815–824.

48 K. M. Meek and Y. A. Elabd, *Macromolecules*, 2015, **48**, 7071–7084.

49 M. Tomoi, K. Yamaguchi, R. Ando, Y. Kantake, Y. Aosaki and H. Kubota, *J. Appl. Polym. Sci.*, 1997, **64**, 1161–1167.

50 H. Long, K. Kim and B. S. Pivovar, *J. Phys. Chem. C*, 2012, **116**, 9419–9426.

51 Y. Zhao, H. Yu, F. Xie, Y. Liu, Z. Shao and B. Yi, *J. Power Sources*, 2014, **269**, 1–6.

52 Y. Z. Zhuo, A. L. Lai, Q. G. Zhang, A. M. Zhu, M. L. Ye and Q. L. Liu, *J. Mater. Chem. A*, 2015, **3**, 18105–18114.

53 L. Wu, Q. Pan, J. R. Varcoe, D. Zhou, J. Ran, Z. Yang and T. Xu, *J. Membr. Sci.*, 2015, **490**, 1–8.

13948 | *J. Mater. Chem. A*, 2016, **4**, 13938–13948

This journal is © The Royal Society of Chemistry 2016